



## Preparation of N-TiO<sub>2</sub> photocatalyst by sol–gel method and its photodegradation of ionic dyes under sunlight

Jing Guo\*, Jiankun Wang\*, Xiaodong Jiang

School of Textile Science and Engineering, TIANGONG UNIVERSITY, Tianjin 300387, China, emails: 17622730360@163.com (J. Guo), jiankunwang@tiangong.edu.cn (J. Wang), 302989953@qq.com (X. Jiang)

Received 23 May 2021; Accepted 13 August 2021

---

### ABSTRACT

In this paper, N-TiO<sub>2</sub> photocatalyst was prepared by the sol–gel method based on alcoholysis with butyl TNBT and urea as raw materials. The N-TiO<sub>2</sub> samples were characterized by X-ray powder diffraction (XRD), X-ray photoelectron spectroscopy (XPS) and UV-Vis diffuse reflectance spectroscopy (DRS). The XRD patterns showed that the crystal structure of anatase was gradually formed and improved when the calcination temperature rose from 350°C to 500°C. When the calcination temperature exceeded 500°C, rutile began to appear. The XPS results explained that the N element was contained in the surface chemical composition of the N-TiO<sub>2</sub>, and the N element was lost with the increase of calcination temperature. The appearance of the N–Ti bond in the Fourier-transform infrared spectrum also suggests that the N element have been incorporated into the TiO<sub>2</sub> lattice. According to the analysis of UV-Vis DRS, the bandgap of the sample obtained by the Tauc plot method at 500°C was 2.56 eV, which was capable of photocatalysis under visible light. The photocatalytic degradation performance of the N-TiO<sub>2</sub> was studied with cationic Golden Yellow X-GL dye (X-GL) and reactive Golden Yellow SNE dye (SNE) as target pollutants. The results showed that the N-TiO<sub>2</sub> had significant photocatalytic degradation performance under sunlight, and could degrade most of the dyes in solution. The total organic carbon of X-GL and SNE dye solution significantly decreased after photocatalytic degradation.

*Keywords:* Sol–gel method; N-TiO<sub>2</sub>; Dye; Sunlight; Photodegradation

---

### 1. Introduction

Water resources are the cornerstone of the earth's ecosystem [1], and “water is life” has become the consensus of mankind [2]. As early as 1927, Hoover Herbert, an American Scholar, put forward that using water scientifically could bring a wealth harvest and happiness of life. For human beings [3], water resources are the basis of food security and disease prevention [4], involving all aspects of life, such as agricultural irrigation, drinking, cooking, and cleaning [5,6]. In addition, the importance of water resources has penetrated social and economic development. In 2010, the United Nations established the issue of water

resources as a human right [7]. Public health, urbanization and industrialization are all affected by water resources. For wild animals, water is both a resource and a habitat. Therefore, water resources are the material basis for the sustainable development of the world.

With the accelerating process of industrialization, a large number of industrial wastewater containing harmful substances has been discharged, the natural environment has been seriously damaged, human health has been threatened unprecedentedly [8], and various new diseases are continuously emerging [9]. Therefore, effective purification of industrial wastewater has become a necessary condition for harmonious coexistence between human beings and nature. About 10,000 tons of dyes are used in

---

\* Corresponding authors.

the textile printing and dyeing industry every year [10]. The dye discharged along with printing and dyeing wastewater accounts for 2%–20%, so it leads to high chroma and poor biodegradability of the wastewater. This causes water pollution and even soil pollution, threatening human production and life [11,12]. Therefore, dye pollution in water has become a major environmental problem.

In the process of printing and dyeing, dyes cannot be completely adsorbed on the fabric surface, and some dyes are discharged with wastewater [13]. The loss of dyes mainly depends on the type of dyes used, ranging from 2% of basic dyes to 50% of reactive dyes [14]. Most synthetic dyes are toxic, which will cause eutrophication of the water body and serious damage to the environment after being discharged with wastewater. Dye molecules prevent sunlight from shining into a water body, which leads to the decrease of dissolved oxygen in the water and the increase of biological oxygen demand, thus breaking the balance of the ecosystem. In addition, azo dyes are carcinogenic and will pose a serious threat to human health, animals and plants [15,16]. Generally, water, sunlight, soap, oxidant, and ordinary microorganisms cannot fade or degrade dyes. The activated sludge method of conventional domestic water has little effect on dye wastewater treatment. Removing stubborn dye molecules from wastewater requires special treatment methods.

Photocatalysis is a new type of water pollution treatment technology. Under the irradiation of ultraviolet light, the semiconductor photocatalyst generates hydroxyl radicals in the aqueous solution, thereby mineralizing the organic pollutants in the solution and purifying the water [17]. Among many semiconductor photocatalysts,  $\text{TiO}_2$  is considered to be a very promising and environmentally friendly photocatalytic material in the field of environmental pollution control because of its high activity, safety, nontoxicity, chemical corrosion, photo corrosion, and low cost [18]. However, its bandgap is 3.2 eV, and it can only play a role under the excitation of ultraviolet light [19,20].  $\text{TiO}_2$  was modified to make full use of the visible light part of the sunlight. Studies have shown that doping

with nonmetallic N element can reduce the bandgap of  $\text{TiO}_2$  and improve its photocatalytic activity. Jung et al. [21] prepared the N-doped  $\text{TiO}_2$  by graft polymerization and pointed out that the degradation rate of methyl orange under visible light was higher than that of  $\text{TiO}_2$ . Cheng et al. [22] synthesized N-doped  $\text{TiO}_2$  by hydrolysis precipitation method and compared its degradation effect on phenol under visible light with pure  $\text{TiO}_2$  and commercial P25  $\text{TiO}_2$ . The results showed that the photocatalytic activity of N-doped  $\text{TiO}_2$  was 2.08 and 1.97 times that of pure  $\text{TiO}_2$  and P25  $\text{TiO}_2$ , respectively. The above studies have shown that doping  $\text{TiO}_2$  with nonmetallic N elements can improve its photocatalytic activity and make full use of visible light.

When  $\text{TiO}_2$  is excited by photons with energy greater than or equal to the bandgap width ( $E_g$ ), electrons ( $e^-$ ) and holes ( $h^+$ ) are generated. Their further reaction paths are shown as A, B, C and D in Fig. 1. First, the photogenerated  $e^-$  transitions from the valence band (VB) to the conduction band (CB), producing an  $h^+$  in VB to form an  $h^+e^-$  pair. Subsequently,  $e^-$  and  $h^+$  react differently during their respective migration processes. The  $e^-$  and  $h^+$  migrate to the surface of the  $\text{TiO}_2$  or inside the  $\text{TiO}_2$ , and surface recombination or internal recombination occurs. This process is called de-excitation and releases heat (A and B). The recombination of the  $e^-$  and  $h^+$  cannot play their own role in the photocatalytic reaction system. After the effective separation of the  $e^-$  and  $h^+$ , they transfer to the surface of the  $\text{TiO}_2$ . The  $h^+$  reacts with the molecules adsorbed on the surface that can accept  $e^-$  to generate hydroxyl radicals  $\cdot\text{OH}$  (C). The dissolved oxygen can absorb electrons, forming  $\cdot\text{O}_2^-$ . The  $h^+$  reacts with molecules adsorbed on the surface that can provide  $h^+$  to produce  $\cdot\text{OH}$  (D). In theory,  $\cdot\text{OH}$  and  $\cdot\text{O}_2^-$  can destroy the molecular structure of various organic compounds in an aqueous solution, mineralize them into  $\text{CO}_2$  and  $\text{H}_2\text{O}$ , and achieve the effect of purifying water [20,23].

After the N element enters the  $\text{TiO}_2$  lattice, a new intermediate energy level will be formed, that is, a new VB of  $\text{N}_{2p}$  will appear above the VB of  $\text{O}_{2p}$ . The emergence of this VB will eventually reduce the  $E_g$  of  $\text{TiO}_2$  ( $E_g < 3.2$  eV) and transfer the light absorption to the visible light region [24].

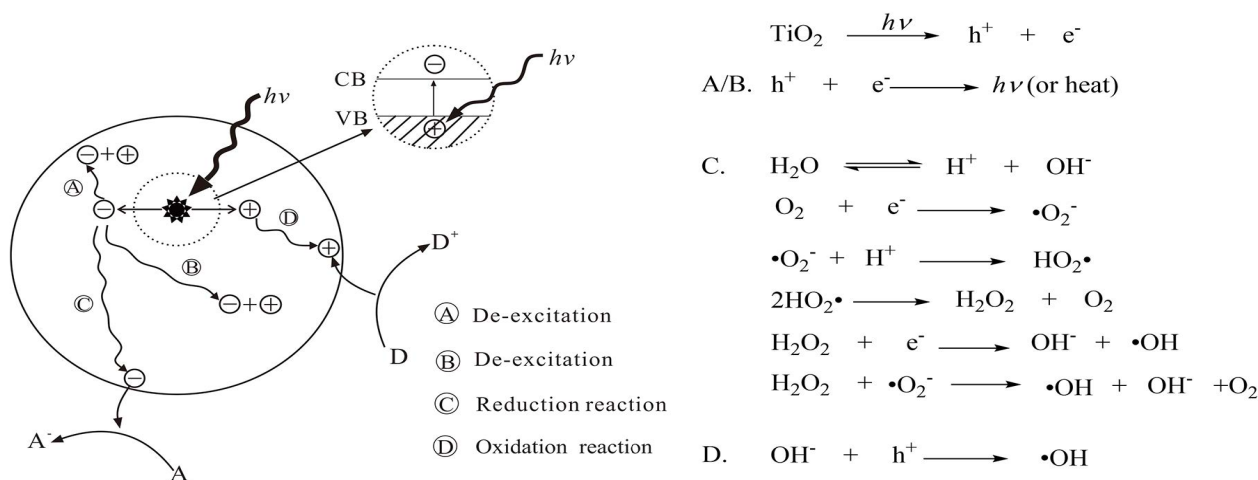


Fig. 1. Photocatalytic reaction mechanism of the  $\text{TiO}_2$ .

When irradiated with visible light,  $e^-$  migrates from VB to CB. Therefore, the N-TiO<sub>2</sub> photocatalyst has higher photocatalytic activity. Based on the above content, TNBT and urea were used as Ti source and N source respectively in this study, and the N-TiO<sub>2</sub> photocatalyst was prepared by sol-gel method based on alcoholysis. The effects of the calcination on the color, crystal form, N element content and bandgap of the samples are studied. With the ionic dyes Golden Yellow X-GL (X-GL) and Golden Yellow SNE (SNE), which are currently widely used in the textile industry, as the target pollutants, the influences of the calcination temperature, N doping amount and pH on photocatalytic degradation performance were tested. The kinetics of photocatalytic degradation and regeneration performance of the N-TiO<sub>2</sub> photocatalyst were also investigated.

## 2. Materials and methods

### 2.1. Chemicals

Butyl titanate (TNBT) was purchased from Tianjin Damao Chemical Reagent Factory, Tianjin, China. Urea was purchased from Tianjin Kemiou Chemical Reagent Co., Ltd., Tianjin, China. Anhydrous ethanol was purchased from Tianjin Fuyu Fine Chemical Co., Ltd., Tianjin, China. Glacial acetic acid was purchased from Tianjin Beifang Tianyi Chemical Reagent Factory, Tianjin, China. X-GL with the maximum absorption wavelength of 440 nm and SNE with the maximum absorption wavelength of 417 nm were supported by Shanghai Rude Dyestuff Chemical Co., Ltd., Shanghai, China and Jiangsu Shenxin Dyestuff Chemical Co., Ltd., by Share Ltd., Jiangsu, China, respectively. The chemical structures are shown in Fig. 2. All chemical reagents were analytically pure and every aqueous solution used in this study was prepared with distilled water.

### 2.2. Preparation of the N-TiO<sub>2</sub> photocatalyst

The N-TiO<sub>2</sub> photocatalyst was prepared by the sol-gel method based on alcoholysis at 25°C. First, 10 mL of

TNBT was added to 30 mL of anhydrous ethanol and was stirred vigorously by mechanical stirring for 30 min. Then, 2 mL of glacial acetic acid as an inhibitor was added to the above-mixed solution and stirred vigorously for 30 min. Subsequently, according to a certain molar ratio of N/Ti, 1 M urea solution prepared with 80% ethanol was added and stirred for 3 h to form sol N-TiO<sub>2</sub>. The sol N-TiO<sub>2</sub> was aged in the natural environment for 48 h to form gel N-TiO<sub>2</sub>. The gel N-TiO<sub>2</sub> was dried in an oven at 80°C for 24 h, and then ground. Finally, the products were calcined in a muffle furnace for 3 h at high temperature. The preparation flow chart of the N-TiO<sub>2</sub> photocatalyst is shown in Fig. 3.

### 2.3. Characterization of the N-TiO<sub>2</sub> photocatalyst

X-ray powder diffraction (XRD) patterns were collected using a Bruker D8 ADVANCE diffractometer (Germany). The samples were scanned from the diffraction angle  $2\theta$  of 5° to 80° with a step size of 0.02°. The surface chemical composition was analyzed by X-ray photoelectron spectroscopy (XPS, Thermo Fisher Scientific, China). Fourier-transform infrared spectrum was carried out by diffused reflectance using a Nicolet iS10 spectrometer Fourier-transform infrared spectroscopy (FTIR, Thermo Fisher Scientific, China). The light absorption performance of the samples was analyzed by UV-Vis diffuse reflectance spectroscopy (DRS; Analytik Jena, Germany), the absorption wavelength range was from 250 to 600 nm, and the bandgap of the samples was measured by the Tauc plot method.

### 2.4. Photodegradation experiment

The photodegradation experiment was carried out in the CEL-LAB500 Photochemical Reactor (Zhongjiao Jinyuan, China) equipped with a xenon lamp (500 W). Then, 0.01 g of the N-TiO<sub>2</sub> photocatalyst was added into a quartz test tube with 20 mL of dye solution (10 mg L<sup>-1</sup>). Throughout the photodegradation experiment, the suspensions were stirred. The effects of the calcination

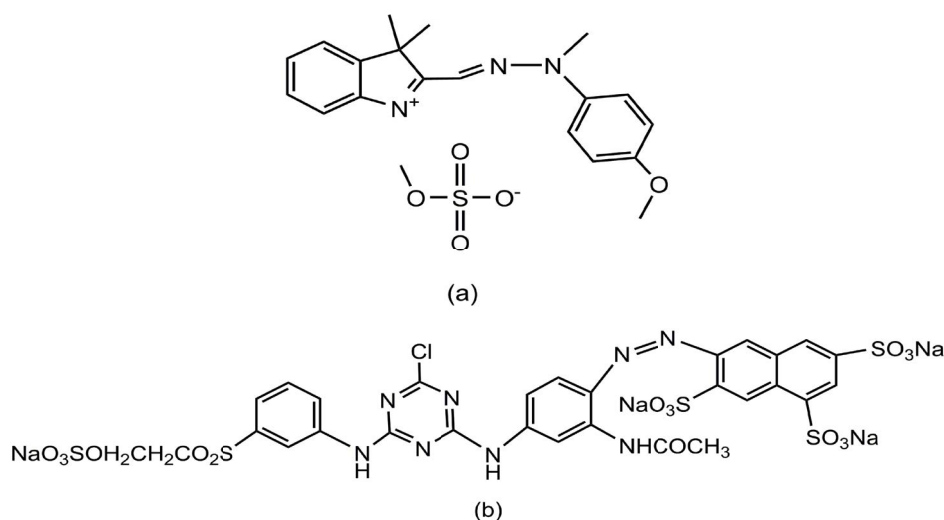


Fig. 2. The chemical structures of (a) Golden Yellow X-GL and (b) Golden Yellow SNE.

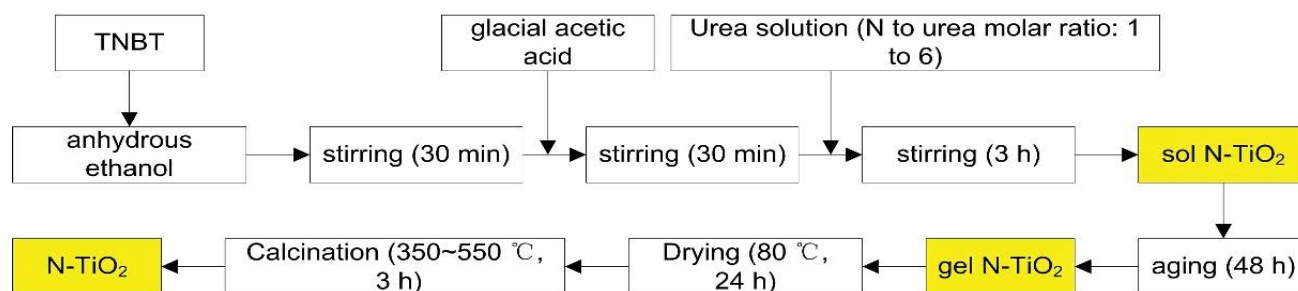


Fig. 3. The preparation flow chart of the N-TiO<sub>2</sub> photocatalyst.

temperature, N content, pH of the dye solution and illumination time (10–60 min) on the removal of the dye were investigated. After the photodegradation experiment, the suspensions were filtered with a 0.22 μm filter, and the dye concentration in the filtrate was measured by an Evolution 201 ultraviolet-visible spectrophotometer (Thermo Fisher Scientific, US). The removal rate of the dye by the N-TiO<sub>2</sub> photocatalyst is as follows:

$$R\% = \frac{C_0 - C_t}{C_0} \times 100 \quad (1)$$

where  $C_0$  and  $C_t$  are the concentrations of the dye initially and at time  $t$ , respectively.

### 3. Results and discussion

#### 3.1. Color of the samples

It can be seen from Fig. 4 that the color of N-TiO<sub>2</sub> photocatalysts was affected by the calcination temperature and  $n(N/Ti)$ . When the  $n(N/Ti)$  was 1.5, as the temperature rose from 350°C to 550°C, the color of the N-TiO<sub>2</sub> photocatalysts gradually changed from black to light yellow, which was mainly due to the presence of the precursor TNBT and urea residues after carbonization on the surface of the samples obtained at lower temperatures. When the calcination

temperature was 500°C, the color of the samples changed from light yellow to dark yellow gradually with the increase of  $n(N/Ti)$  and the enhancement of yellow was mainly caused by the increase of nitrogen content in the samples.

#### 3.2. Crystal properties

It can be found from Fig. 5 that the calcination temperature had an important influence on the crystal form of the N-TiO<sub>2</sub> photocatalyst. As the temperature rose, the crystal structure of anatase gradually formed and improved. The diffraction peaks at 25.39°, 36.90°, 37.83°, 38.46°, 48.02°, 53.90°, 55.06°, 62.73°, and 68.77° from the sample obtained at 500°C were corresponded to (101), (103), (004), (112), (200), (105), (211), (204), (116), (220), (215) and (301) characteristic crystal planes of anatase TiO<sub>2</sub> [25]. When the calcination temperature exceeded 500°C, rutile began to appear. The diffraction peaks at 27.43°, 36.18°, 41.30°, 44.10°, 54.34°, 56.61°, and 63.97° corresponded to the (110), (101), (111), (210), (211), (220), and (310) characteristic crystal planes of rutile TiO<sub>2</sub> [26].

#### 3.3. Surface chemical composition analysis

In order to study the influence of the calcination temperature on N content, the XPS spectra of samples at 400°C,

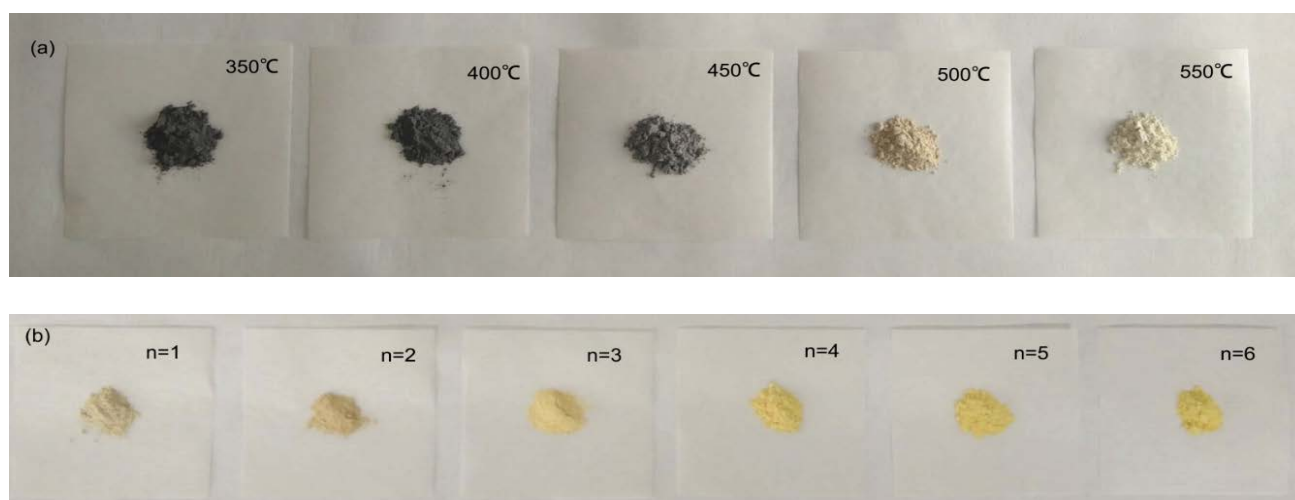


Fig. 4. (a) The N-TiO<sub>2</sub> photocatalysts obtained at different calcination temperatures and (b) The N-TiO<sub>2</sub> photocatalysts with different  $n(N/Ti)$ .

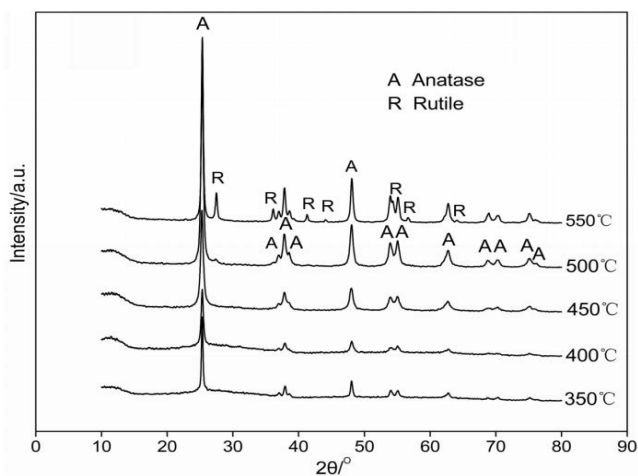


Fig. 5. XRD spectra of the N-TiO<sub>2</sub> photocatalysts were obtained at different calcination temperatures.

450°C and 500°C were tested respectively. The results showed that with the increase of the calcination temperature, the N content decreased, as shown in Table 1, indicating that the increase of the calcination temperature caused N loss to a certain extent. The full XPS spectrum of the N-TiO<sub>2</sub> photocatalyst obtained at 500°C and the high-energy resolution spectra of the titanium, oxygen and nitrogen elements are shown in Fig. 6. On the one hand, it can be seen from the full spectrum that there were Ti, O, N and C elements and the C element may be caused by incomplete removal of the precursor at 500°C. On the other hand, the chemical environment in which elements existed can be seen from the high-energy resolution spectra. Fig. 6b shows the high-energy resolution spectrum of Ti 2p, and the peaks at 464.2 and 458.5 eV were the characteristic peaks of Ti 2p<sub>1/2</sub> and Ti 2p<sub>3/2</sub>, respectively [27]. Fig. 6c shows the high-energy resolution spectrum of O 1s and it can be found that there were two kinds of oxygen elements in the sample, which were the Ti–O bond of TiO<sub>2</sub> or O<sup>2-</sup> and –OH. As displayed in Fig. 6d, two peaks at 400.9 and 399.2 eV respectively represented the characteristic peaks of Ti–O–N and Ti–N bond [28] and the existence of the N 1s peak indicated that nitrogen successfully entered the crystal lattice of TiO<sub>2</sub> during the synthesis process.

### 3.4. UV-Vis DRS analysis

The bandgap  $E_g$  (eV) of the samples were calculated by the Tauc plot method. According to Eq. (2), the tangent line was made for the inflection point of the curve. The intersection point of tangent and  $x$ -axis was  $E_g$  of the sample [29], as shown in Fig. 7b.

$$(\alpha h\nu)^{1/n} = A(h\nu - E_g) \quad (2)$$

$$h\nu = \frac{hc}{\lambda}$$

where  $\alpha$  is the absorbance index. The absorbance index is directly proportional to the absorbance (Abs). No matter

Table 1  
N content of samples calcined at different temperatures

Calcination temperature (°C)	N content (%)
400	1.79
450	1.31
500	1.13

whether Abs or  $\alpha$  is used, there is no effect on  $E_g$ , and only the coefficient  $A$  is different. Therefore, Abs is directly used instead of  $\alpha$ .  $h$  is the Planck constant with the value of  $6.63 \times 10^{-34}$  J s,  $\nu$  is the frequency, and  $c$  is the speed of light with the value of  $3 \times 10^8$  m s<sup>-1</sup>.  $n$  is related to the type of semiconductor. The  $n$  values of direct bandgap semiconductor and indirect bandgap semiconductor are 1/2 and 2 respectively. In this study, the  $n$  value of TiO<sub>2</sub> is 1/2.

In this project, there were a lot of residual carbides on the surface of the N-TiO<sub>2</sub> photocatalysts obtained at 350°C–450°C, which could absorb visible light without the photocatalytic effect. Therefore, only for the samples obtained at 500°C and 550°C, the bandgaps calculated through the Tauc plot method were 2.56 and 2.63 eV respectively, while that of commercial TiO<sub>2</sub> was 3.2 eV. It followed that the bandgap of the N-TiO<sub>2</sub> photocatalyst prepared in this paper was significantly reduced, and the N-TiO<sub>2</sub> photocatalyst had photocatalytic ability under visible light. The bandgap of the sample obtained at 550°C was higher than that at 500°C. On the one hand, the loss of N was more serious at a higher temperature. On the other hand, the crystal form of TiO<sub>2</sub> transformed from anatase to rutile at a higher temperature. These two reasons led to the difference in the bandgap.

### 3.5. FTIR analysis

Fig. 8 displays the FTIR spectrum of the N-TiO<sub>2</sub> photocatalyst with  $n(N/Ti)$  of 3 calcined at 500°C. For the FTIR spectrum, the strong band located at 500 cm<sup>-1</sup> was attributed to Ti–O stretching mode. The bands at around 1,480 and 1,240 cm<sup>-1</sup> were attributed to the vibrations of the Ti–N bond, while the band at 1,385 cm<sup>-1</sup> could be ascribed to the vibration of the N–O bond [30]. The peak at around 1,645 cm<sup>-1</sup> corresponded to the bending vibrations of O–H and the broadband at 3,400 cm<sup>-1</sup> observed in the spectrum could be ascribed to surface hydroxyl groups and absorbed water molecules. The appearance of the N–Ti bond in the sample suggests that the N element have been incorporated into the TiO<sub>2</sub> lattice. This finding is in accordance with the XPS results previously discussed.

### 3.6. Photodegradation properties of the N-TiO<sub>2</sub> photocatalyst

#### 3.6.1. Effect of the calcination temperature on photodegradation of the N-TiO<sub>2</sub> photocatalyst

The samples with the  $n(N/Ti)$  of 1.5 and the calcination temperature of 350°C–550°C were used for photodegradation of X-GL and SNE in a photochemical reactor for 60 min. The experimental results were shown in Fig. 9. With the increase of the calcination temperature,

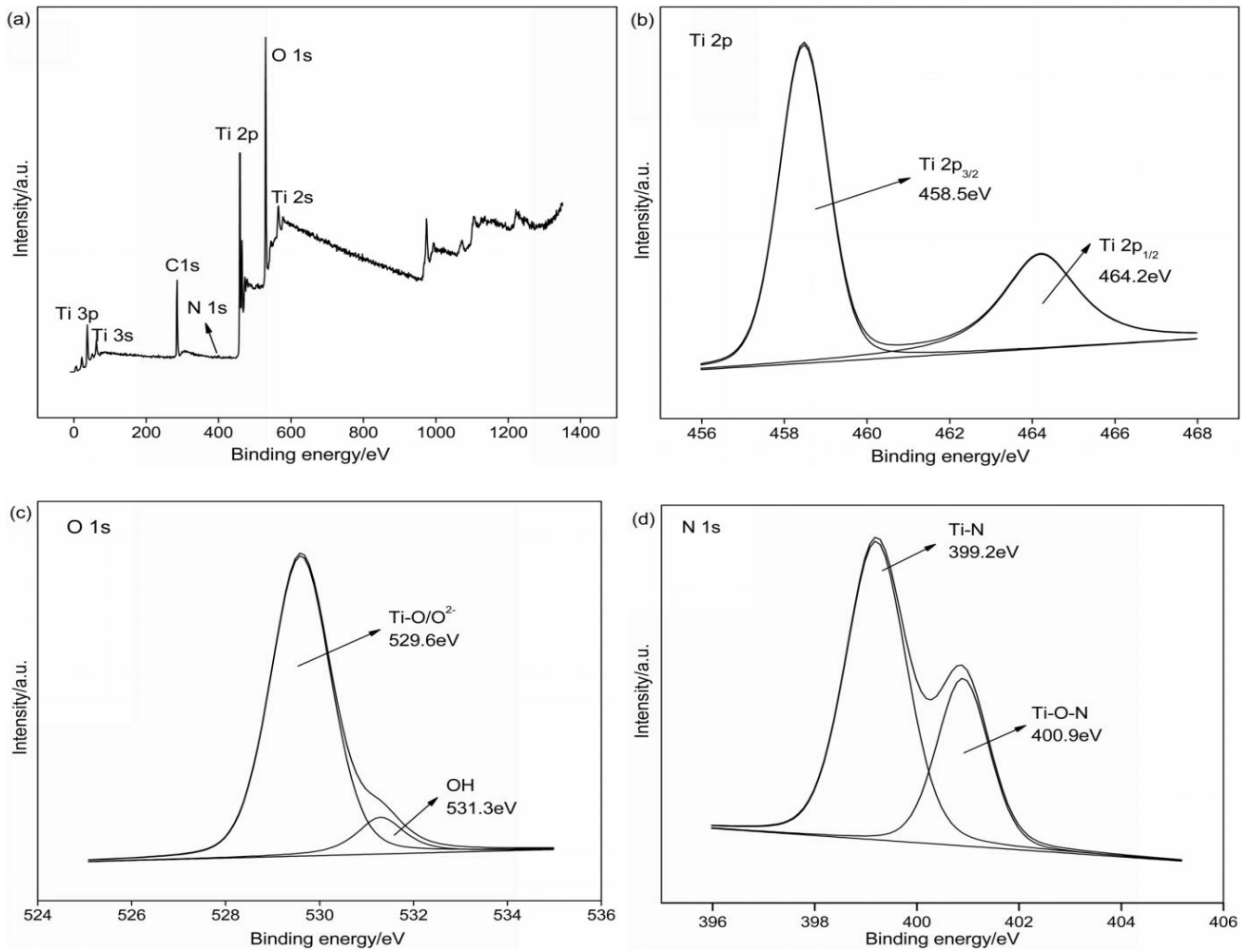


Fig. 6. XPS spectra of the N-TiO<sub>2</sub> photocatalyst calcined at 500°C.

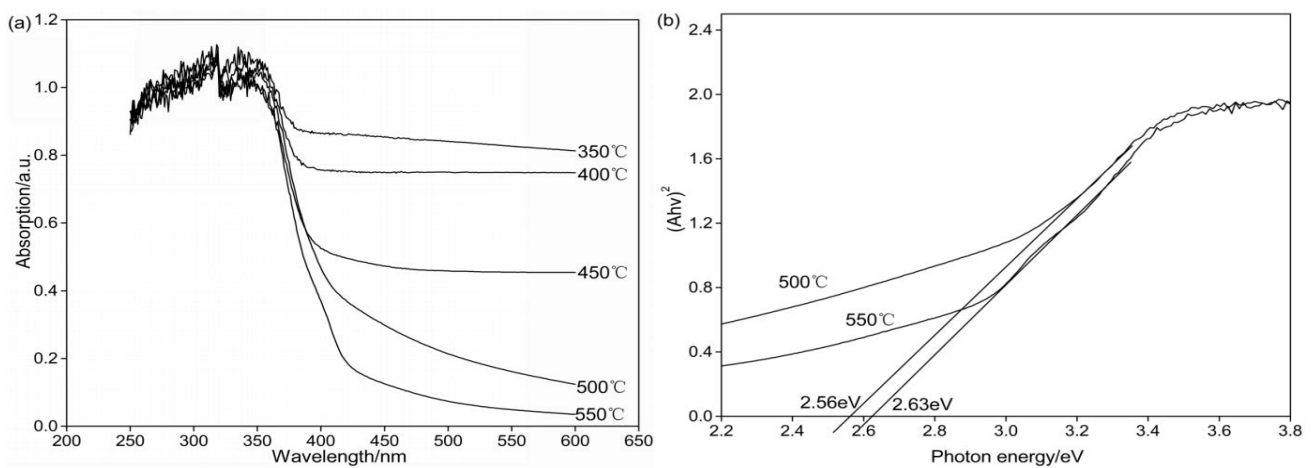


Fig. 7. UV-Vis diffuse reflectance spectroscopy (a) and bandgaps (b) of the samples.

the photodegradation rate of X-GL and SNE gradually increased. When the calcination temperature was 500°C, the photodegradation rate reached the highest and decreased slightly at 550°C. The above phenomenon was

mainly caused by two reasons. On the one hand, as we all know that the anatase TiO<sub>2</sub> has better photocatalytic performance. The XRD analysis showed that the calcination temperature was a key factor in the formation of the crystal

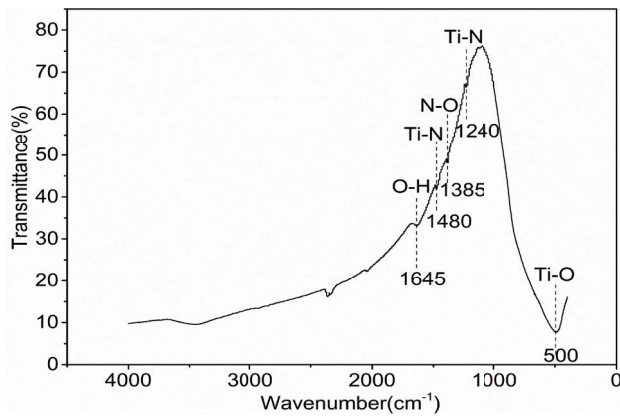


Fig. 8. FTIR spectrum of the N-TiO<sub>2</sub> photocatalyst with n(N/Ti) of 3 calcined at 500°C.

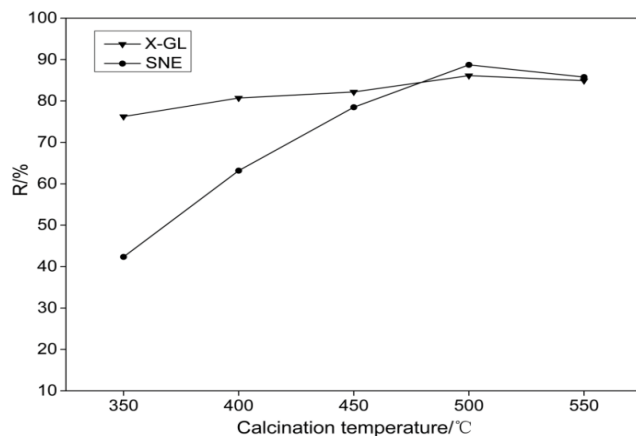


Fig. 9. Effect of the calcination temperature on photodegradation of Golden Yellow X-GL and Golden Yellow SNE by N-TiO<sub>2</sub>.

form of the sample, and the crystal structure of anatase was gradually formed and improved when the calcination temperature rose from 350°C to 500°C. When the calcination temperature exceeded 500°C, rutile began to appear. On the other hand, UV-Vis DRS showed that the sample obtained at 500°C had higher N content and a lower bandgap. In conclusion, the N-TiO<sub>2</sub> photocatalyst obtained at 500°C had the best photocatalytic effect.

### 3.6.2. Effect of n(N/Ti) on photodegradation of the N-TiO<sub>2</sub> photocatalyst

The effect of N doping content on the photodegradation rates of dyes is shown in Fig. 10. The illumination time of this group of experiments was 40 min. When the n(N/Ti) increased from 1 to 3, the photodegradation rates of dyes reached the maximum. With the further increase of N doping amount, the removal rate began to decrease. N element can replace the O element in the TiO<sub>2</sub> lattice in a small amount to narrow the bandgap, which made it have visible-light activity. Therefore, with increasing n(N/Ti), the photodegradation rates of dyes under xenon light increased. When the amount of N doping was

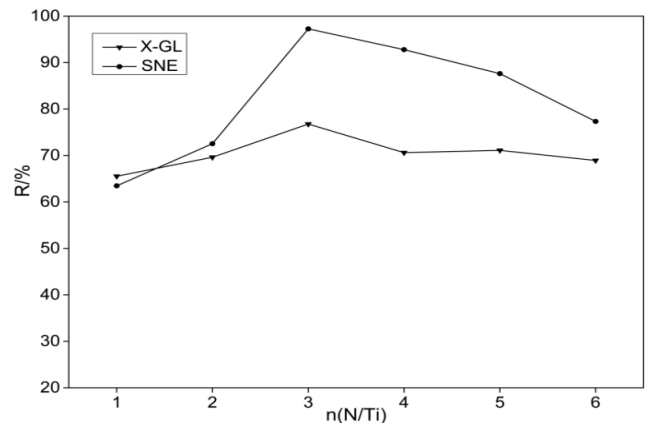
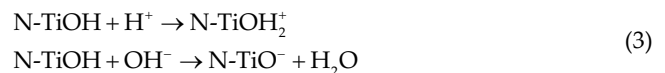


Fig. 10. Effect of N content on photodegradation of Golden Yellow X-GL and Golden Yellow SNE by N-TiO<sub>2</sub>.

too high, the proportion of TiO<sub>2</sub> decreased too much, resulting in the relative reduction electron-hole pairs, which next affected the photocatalytic efficiency of N-TiO<sub>2</sub>. This may cause the photodegradation rates of dyes reduced. Therefore, the optimum n(N/Ti) was 3.

### 3.6.3. Effect of pH on photodegradation of the N-TiO<sub>2</sub> photocatalyst

The isoelectric point (pH<sub>pzc</sub>) of the N-TiO<sub>2</sub> photocatalyst was determined by the pH drift method. 50 mL of 0.01 M NaCl solution was taken and the initial pH (pH<sub>i</sub>) of the solution was adjusted from 4 to 10 by 0.1 M HCl or NaOH. Subsequently, 0.15 g of N-TiO<sub>2</sub> was added to the solution with different pH and stirred at 25°C. After stirred for 48 h, the final pH (pH<sub>f</sub>) of the solution was measured. The results were shown in Fig. 11. The pH<sub>pzc</sub> of N-TiO<sub>2</sub> was 6.81. According to the literatures, when the pH value of the solution is lower than pH<sub>pzc</sub>, the surface of N-TiO<sub>2</sub> is positively charged. Conversely, the surface of N-TiO<sub>2</sub> is negatively charged [31]. This phenomenon can be explained by Eq. (3). When there is a large amount of H<sup>+</sup> or OH<sup>-</sup> in the solution, N-TiO<sub>2</sub> is ionized and charged with positive or negative charges respectively, thus affecting the enrichment of dyes. Therefore, in the subsequent photodegradation experiment, the pH of the X-GL solution was adjusted to 8, and the pH of the SNE solution was adjusted to 6.



### 3.6.4. Effect of time on photodegradation of the N-TiO<sub>2</sub> photocatalyst

The Langmuir–Hinshelwood (L-H) kinetic model is usually used as a standard model to describe the photodegradation behavior of dyes [32,33]. The simplified expression of the L-H kinetic model is as follows:

$$\ln\left(\frac{C_0}{C_t}\right) = kt \quad (4)$$

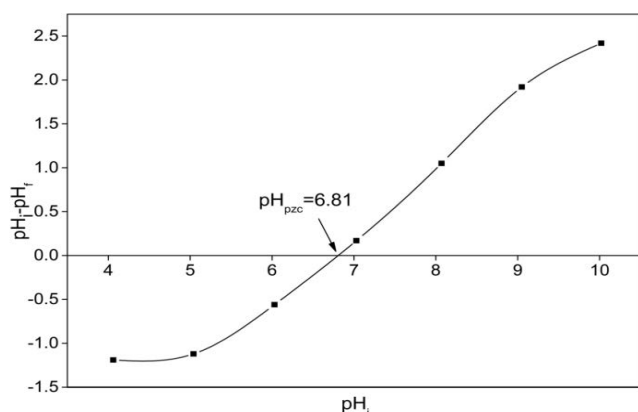


Fig. 11. Effect of pH on photodegradation of Golden Yellow X-GL and Golden Yellow SNE by N-TiO<sub>2</sub>.

where  $k$  is the reaction rate constant ( $\text{min}^{-1}$ ) and  $t$  is the irradiation time ( $\text{min}$ ).

To study the photodegradation kinetics of X-GL and SNE dyes by N-TiO<sub>2</sub>, the experimental data were analyzed by linear regression, and the results are shown in Fig. 12 and Table 2. From the values of correlation coefficient  $R^2$  exceeding 0.99, it can be concluded that the photodegradation behavior of X-GL and SNE dyes by N-TiO<sub>2</sub> followed the L-H kinetic model. The reaction rates of photodegradation of X-GL and SNE were 0.03745 and 0.05154  $\text{min}^{-1}$  respectively, indicating that the degradation of SNE was faster. This was mainly due to the lower absorbance and lighter color of SNE solution than those of X-GL solution with the same concentration, which was more conducive to light entering the solution and facilitating the reaction.

### 3.6.5. Analysis of total organic carbon

To preliminary study, the photodegradation process and photodegradation effect of the prepared N-TiO<sub>2</sub> on X-GL and SNE dyes, the total organic carbon (TOC) of X-GL or SNE dye solution was tested after reacting under simulated sunlight for 40 min. The results are shown in Fig. 13. It can be found that the TOC greatly reduced both X-GL solution and SNE solution, indicating that the dyes were indeed mineralized and converted into inorganic carbon after photodegradation by N-TiO<sub>2</sub>. However, compared with the photodegradation rates of X-GL and SNE after illumination for 40 min in section 3.5.2, the decrease of TOC was less than that of dye concentration, indicating that the dye was first degraded into small molecular organics before it was completely mineralized, and intermediate products were produced in the degradation process. Therefore, it is

Table 2  
Parameters of Langmuir–Hinshelwood kinetic model for Golden Yellow X-GL and Golden Yellow SNE by N-TiO<sub>2</sub>

Dyes	$k$	$R^2$
Golden Yellow X-GL	0.03745	0.9981
Golden Yellow SNE	0.05154	0.9962

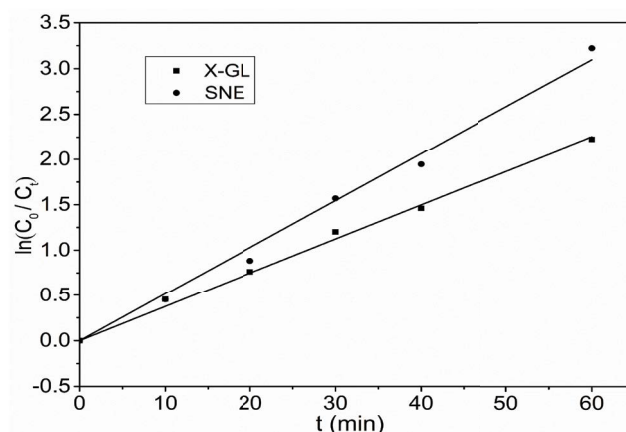


Fig. 12. Linear fits of Langmuir–Hinshelwood kinetic model for Golden Yellow X-GL and Golden Yellow SNE by N-TiO<sub>2</sub>.

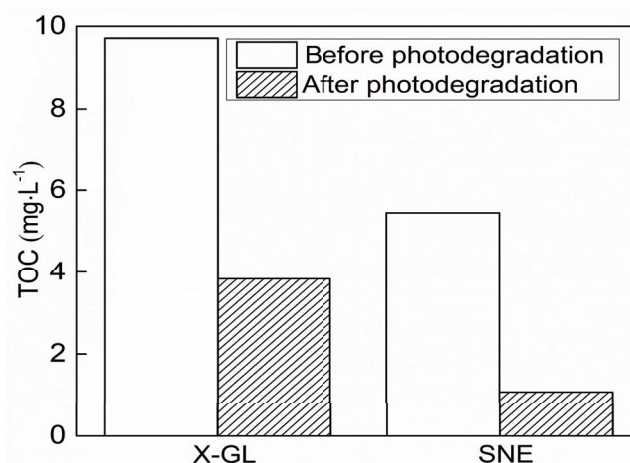


Fig. 13. TOC of Golden Yellow X-GL and Golden Yellow SNE solution before and after the photodegradation by N-TiO<sub>2</sub>.

preliminarily inferred that the mechanism for photodegradation of X-GL and SNE by N-TiO<sub>2</sub> is shown in Fig. 14.

### 3.6.6. Reusability studies

The reusability of photocatalytic materials is an important factor for their performance in dye treatment. The X-GL or SNE solution containing N-TiO<sub>2</sub> was irradiated under the xenon lamp for 60 min to study the reusability of N-TiO<sub>2</sub>. After each cycle test, N-TiO<sub>2</sub> was soaked and cleaned with 80% ethanol solution to remove residual dyes on the surface and avoid the combination of undegraded dyes with active sites on the surface of N-TiO<sub>2</sub>, which would cause photocatalyst poisoning and reduce photocatalytic activity. The results of four cycles are shown in Fig. 15. The results showed that the removal rates of dyes decreased with the increase of cycle times, but the removal rates of X-GL and SNE could reach more than 80% after four cycles, which indicated that the N-TiO<sub>2</sub> prepared in this project had good regeneration performance and was of great significance to reduce the treatment cost of dye wastewater.

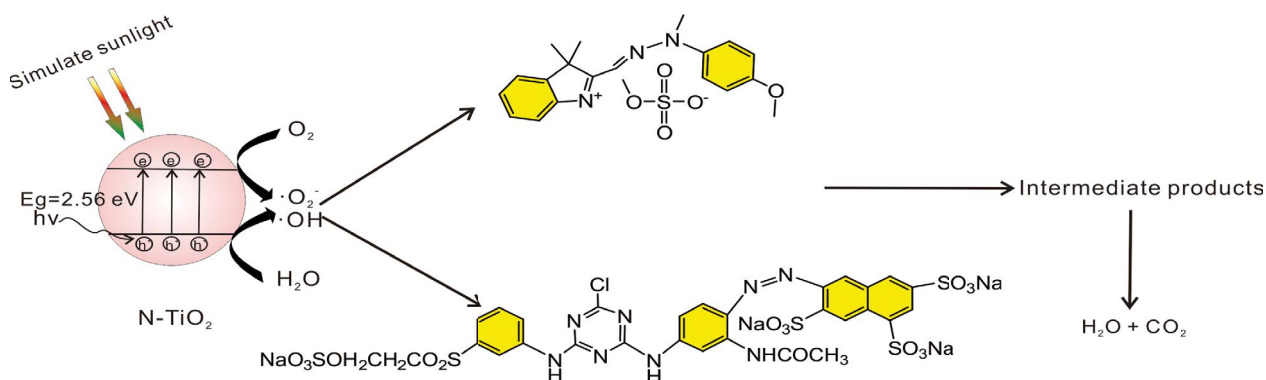


Fig. 14. The figure of mechanism for photodegradation of Golden Yellow X-GL and Golden Yellow SNE by N-TiO<sub>2</sub>.

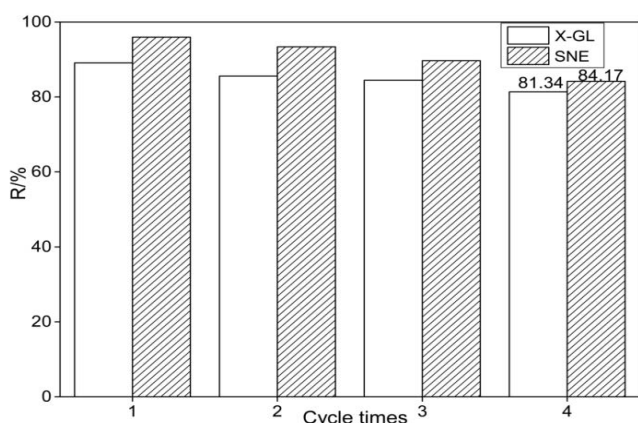


Fig. 15. Reusability efficiency of N-TiO<sub>2</sub> for Golden Yellow X-GL and Golden Yellow SNE removal.

#### 4. Conclusions

Through the XRD, XPS, FTIR and UV-Vis analysis, the anatase N-TiO<sub>2</sub> photocatalyst with high photocatalytic activity can be synthesized successfully by the sol-gel method based on alcoholysis, and its  $pH_{pzc}$  was 6.81 measured by the pH drift method. The calcination temperature and doping amount of the N element are important factors affecting the photocatalytic efficiency of N-TiO<sub>2</sub>. The samples with n(N/Ti) of 3 calcined at 500°C had the highest photodegradation rates for X-GL and SNE. The kinetics study showed that the photodegradation of X-GL and SNE by N-TiO<sub>2</sub> followed the L-H model, and the reaction rates of X-GL and SNE were 0.03745 and 0.05154 min<sup>-1</sup>, respectively. At the same time, N-TiO<sub>2</sub> had a good recycling performance. After four times of recycling, the removal rates of X-GL and SNE can reach more than 80%. The N-TiO<sub>2</sub> photocatalyst has a good application prospect in the field of dye wastewater treatment.

#### References

- Vignieri, Sacha, Fahrenkamp-Uppenbrink, Julia, *Ecosystem Earth, Science*, 356 (2017) 258–259.
- A. John, *Water is the staff of life and at the heart of public health*, *J. R. Soc. Med.*, 112 (2019) 516–518.
- A.L. Bruce, Herbert Hoover, spokesman of humane efficiency: the Mississippi flood of 1927, *Am. Q.*, 22 (1970) 690–700.
- M. Qadir, B.R. Sharma, A. Bruggeman, R. Choukr-Allah, F. Karajeh, Non-conventional water resources and opportunities for water augmentation to achieve food security in water scarce countries, *Agric. Water Manage.*, 87 (2007) 2–22.
- J. Magrath, *Water: A Shared Responsibility*, The United Nations World Water Development Report 2, 2007, pp. 309–311.
- J.D. Priscoli, What is public participation in water resources management and why is it important?, *Water Int.*, 29 (2004) 221–227.
- G. Joyeeta, A. Rhodante, A. Lawal, The human right to water: moving towards consensus in a fragmented world, *Rev. European Commun. Int. Environ. Law*, 19 (2010) 294–305.
- H. Almas, Z. Mahrukh, M. Asim, A. Sana, S. Samia, Assessment of wastewater quality of drains for irrigation, *J. Environ. Prot.*, 4 (2013) 937–945.
- M.M. Mohammad, N. Azam, R.S.A. Hamid, H.M. Amir, Adsorption of cationic dye textile wastewater using Clinoptilolite: isotherm and kinetic study, *J. Text. Inst.*, 110 (2019) 74–80.
- V. Katheresan, J. Kansedo, S.Y. Lau, Efficiency of various recent wastewater dye removal methods: a review, *J. Environ. Chem. Eng.*, 6 (2018) 4676–4697.
- K. Rita, Textile dyeing industry an environmental hazard, *Nat. Sci.*, 4 (2012) 22–26.
- A.K. Tawfik, S.A. Meram, R. Mohamed, Textile dyeing industry: environmental impacts and remediation, *Environ. Sci. Pollut. Res.*, 27 (2019) 3803–3818.
- D.A. Yaseen, M. Scholz, Textile dye wastewater characteristics and constituents of synthetic effluents: a critical review, *Int. J. Environ. Sci. Technol.*, 16 (2019) 1193–1226.
- P.S. Rajat, K.S. Pradeep, L.S. Ram, Present status of biodegradation of textile dyes, *Curr. Trends Biomed. Eng. Biosci.*, 3 (2017) 66–68.
- J. Guo, J. Wang, G. Zheng, X. Jiang, Optimization of the removal of reactive Golden Yellow SNE dye by cross-linked cationic starch and its adsorption properties, *J. Eng. Fibers Fabr.*, 14 (2019) 1–13.
- H.M. Noshaba, Z. Hajira, A. Naeem, Organismic-level acute toxicology profiling of reactive azo dyes, *Environ. Monit. Assess.*, 190 (2018) 612, doi: 10.1007/s10661-018-6986-7.
- M.M. Mphilisi, J.N. Catherine, B.M. Bhekie, Recent developments in environmental photocatalytic degradation of organic pollutants: the case of titanium dioxide nanoparticles—a review, *J. Nanomater.*, 2015 (2015) 1–29, doi: 10.1155/2015/790173.
- J. Guo, J. Wang, G. Zheng, X. Jiang, A TiO<sub>2</sub>/crosslinked carboxymethyl starch composite for high-efficiency adsorption and photodegradation of cationic Golden Yellow X-GL dye, *Environ. Sci. Pollut. Res.*, 26 (2019) 24395–24406.
- Z. Wang, W. Cai, X. Hong, X. Zhao, F. Xu, C. Cai, Photocatalytic degradation of phenol in aqueous nitrogen-doped TiO<sub>2</sub> suspensions with various light sources, *Appl. Catal., B*, 57 (2005) 223–231.

- [20] L. Yao, H. Yang, Z. Chen, M. Qiu, B. Hu, X. Wang, Bismuth oxychloride-based materials for the removal of organic pollutants in wastewater, *Chemosphere*, 273 (2021) 128576, doi: 10.1016/j.chemosphere.2020.128576.
- [21] T.P. Jung, J.K. Dong, H.K. Do, H.K. Jong, A facile graft polymerization approach to N-doped TiO<sub>2</sub> heterostructures with enhanced visible-light photocatalytic activity, *Mater. Lett.*, 202 (2017) 66–69.
- [22] X.W. Cheng, X.J. Yu, Z.P. Xing, Characterization and mechanism analysis of N doped TiO<sub>2</sub> with visible light response and its enhanced visible activity, *Appl. Surf. Sci.*, 258 (2012) 3244–3248.
- [23] M.R.D. Khaki, M.S. Shafeeyan, A.A.A. Raman, M.A.W.D. Wan, Application of doped photocatalysts for organic pollutant degradation – a review, *J. Environ. Manage.*, 198 (2017) 78–94.
- [24] N. Kovalevskiy, D. Selishchev, D. Svintsitskiy, S. Selishcheva, A. Berezin, D. Kozlov, Synergistic effect of polychromatic radiation on visible light activity of N-doped TiO<sub>2</sub> photocatalyst, *Catal. Commun.*, 134 (2020) 105841, doi: 10.1016/j.catcom.2019.105841.
- [25] A. Sanchez-Martinez, O. Ceballos-Sanchez, C. Koop-Santa, E.R. López-Mena, E. Orozco-Guareño, M. García-Guaderrama, N-doped TiO<sub>2</sub> nanoparticles obtained by a facile coprecipitation method at low temperature, *Ceram. Int.*, 44 (2018) 5273–5283.
- [26] M. Tatiana, P. Paraskevi, V. Danae, N-doped TiO<sub>2</sub> photocatalysts for bacterial inactivation in water, *J. Chem. Technol. Biotechnol.*, 93 (2018) 2518–2526.
- [27] X. Liu, Y. Liu, S. Lu, W. Guo, B. Xi, Performance and mechanism into TiO<sub>2</sub>/zeolite composites for sulfadiazine adsorption and photodegradation, *Chem. Eng. J.*, 350 (2018) 131–147.
- [28] G. Yang, Z. Jiang, H. Shi, T. Xiao, Z. Yan, Preparation of highly visible-light active N-doped TiO<sub>2</sub> photocatalyst, *J. Mater. Chem.*, 20 (2010) 5301–5309.
- [29] R. Sunil, R. Swapnil, G. Suja, K.S. Virendra, R.G. Parag, B.P. Aniruddha, Synthesis and characterization of samarium and nitrogen doped TiO<sub>2</sub> photocatalysts for photo-degradation of 4-acetamidophenol in combination with hydrodynamic and acoustic cavitation, *Sep. Purif. Technol.*, 209 (2019) 254–269.
- [30] H. Li, Y. Hao, H. Lu, L. Liang, Y. Wang, J. Qiu, X. Shi, Y. Wang, J. Yao, A systematic study on visible-light N-doped TiO<sub>2</sub> photocatalyst obtained from ethylenediamine by sol–gel method, *Appl. Surf. Sci.*, 344 (2015) 112–118.
- [31] P. Devarly, Y. Kartika, N. Indraswati, Activated carbon from jackfruit peel waste by H<sub>3</sub>PO<sub>4</sub> chemical activation: pore structure and surface chemistry characterization, *Chem. Eng. J.*, 140 (2008) 32–42.
- [32] H. Umma, M.D.S. Islam, A.S. Tawsif, M.A. Amalina, C.A. Bee, Adsorption and photocatalytic degradation of anionic dyes on chitosan/PVA/Na-titanate/TiO<sub>2</sub> composites synthesized by solution casting method, *Carbohydr. Polym.*, 149 (2016) 317–331.
- [33] C.I. Elida, P. Rodica, M. Florica, A.C. Liliana, J. Agnes, O. Corina, R. Cornelia, L. Carmen, S. Paula, Photocatalytic activity of a nitrogen-doped TiO<sub>2</sub> modified zeolite in the degradation of Reactive Yellow 125 azo dye, *J. Taiwan Inst. Chem. Eng.*, 44 (2013) 270–278.